J Mater Sci (2007) 42:7062–7068
DOI 10.1007/s10853-006-1423-7

Synthesis of a soluble polyaniline–ferrite composite: magnetic and electric properties

Juan C. Aphesteguy · Silvia E. Jacobo

Received: 16 August 2006 / Accepted: 11 December 2006 / Published online: 5 May 2007

Abstract We report the preparation of a processible magnetite/polyaniline (Fe_3O_4/PANI) nanocomposite, containing dodecylbencensulfonic acid (DBSA) as a surfactant and dopant, with both magnetic and conducting properties. Different amounts of Fe_3O_4 nanoparticles were successfully disposed with $FeCl_3$ solution to prevent their aggregation in the solution by the application of common ion effect. The magnetic properties of the resulting composites were investigated by a quantum design magnetometer (PMPS). The (Fe_3O_4/PANI) nanocomposite showed at 300 K no loop of hysteresis indicating the superparamagnetic nature. The saturation magnetization varies from 0.167 to 28.45 emu/g with increasing Fe_3O_4 content. Zero field cooling (ZFC) and Field cooling (FC) profiles showed that the polyaniline matrix allows each ferrite nanoparticles to behave independently and interparticle interactions are not important for iron oxide content lower than 36 wt.%. The electrical conductivity of composites was found to be higher than that of the pure PANI in spite of the insertion of the insulating material Fe_3O_4 particles. It is noticeable that conductivity increases with low Fe_3O_4 particles content and then decreases. Structural characterization by X-ray diffraction (XRD), UV spectroscopy and thermogravimetric analysis (TGA) have been performed.

J. C. Aphesteguy · S. E. Jacobo (✉)
LAFMACEL, Facultad de Ingeniería, Universidad de Buenos Aires, Paseo Colón 850, Buenos Aires 1063, Argentina
e-mail: sjacobo@fi.uba.ar

Introduction

The integration of superparamagnetic materials and functional organic materials has attracted an increase interest. Materials having both electrical and magnetic properties are required for the application of electrical and magnetic shielding, molecular electronics, nonlinear optics, sensor and microwave absorbent [1–3].

Earlier studies have also been carried out to make conducting polymer incorporated with ferrite particles [4, 5]. The resulting composites have low room temperature conductivity (10^{-6}–10^{-3} S/cm) and low coercive force ($H_c \approx 0$), and their structures and properties are related to the synthetic method. Nanostructures of polyaniline-magnetite nanoparticles composites were also prepared in the presence of β-naphthalene sulfonic acid (NSA) as a dopant that shows a magnetization value of 6 emu/g [6]. Structural characterization of the PANI composites indicates that the doping of PANI with mineral acids leads to electrical conducting properties of composites, whereas the nanocrystalline magnetic particles are responsible for the observed ferromagnetic properties of composites [7]. We have reported the synthesis of polyaniline with high ferromagnetic properties and moderate conductivity (M_s = 72 emu/g, σ ~10^{-4} S/cm) [8]. Long et al. [9] reported the preparation of Fe_3O_4/PANI nanorods doped with NSA with different iron content. Although the coercive force of these samples is small (H_c = 55–60 Oe), it does not decrease to zero. The reason could be attributed to clustered particles. Chen et al. [10] reported the preparation of polypirrole–Fe_3O_4 nanocomposites by the use of common ion effect with low coercive force and low magnetization. A large amount of Fe^{3+} was absorbed onto the surface of the magnetite nanoparticles and formed positive charged (Fe^{3+}) shell. Consequently, the surface of the magnetite

became the active surface to polymerize aniline monomers. The result composite is not soluble in organic solvents. Recently, several methods have been developed to improve the processibility of PANI by increasing its solubility in various solvents. Cao et al. [11, 12] reported that PANI doped with DBSA or camphor sulfonic acid became soluble in various organic solvents such as chloroform and xylene. This procedure could be used to fabricate a flexible light emitting diode (LED) [13]. A PANI with improved processibility was synthesized via the chemical polymerization in an aqueous solution of DBSA aniline salt (ANIDBSA) and aniline hydrochloric acid (ANIHCl) by Yein and Ruckenstein [14].

In the present paper, the chemical oxidative polymerization of (ANIDBSA) and (ANIHCl) with $FeCl_3$ solution in the presence of Fe_3O_4 nanoparticles was investigated. This pathway was selected, because one expects the ANIDBSA salts moieties the polymer to enhance its solubility, hence the processibility.

Experimental section

Synthesis of magnetite nanoparticles

The magnetic nanoparticles were synthesized by mixing a water solution of $FeCl_2{\cdot}4H_2O$ (1.0 M) and $FeCl_3{\cdot}6H_2O$ (1.5 M). The above mixture was poured in aqueous ammonium solution (50 vol%) and the resulting solution was stirred for 2 h. Ferrite particles are precipitated out, filtered and thoroughly washed with distilled water. Each wash step was carried out until the filtrate became clear and colorless. Finally, the resulting magnetic nanoparticles were disposed by $FeCl_3$ solution by ultrasonic stirring.

Synthesis of magnetite/polyaniline (Fe_3O_4/PANI) nanocomposite

Polyaniline composites were synthesized by using the emulsion method using DBSA in aqueous solution. Fixed concentrations of the Fe_3O_4 nanoparticles prepared by the previous step were added into a 200 ml round-bottom flask equipped with a mechanical stirrer. Aniline monomer was added to the flask containing distilled water, DBSA and HCl in a selected molar ratio (7:3) with a molar ratio of aniline/(DBSA + HCl) =1 [14]. In order to obtain a composite with a higher content of the conductor polymer, an acidic aqueous $FeCl_3$ solution was added, under supersonic stirring, to the reacting solution to polymerize the remained aniline monomer. Then the polymerization was allowed to proceed for 12 h at room temperature under stirring. The products were washed with deionizer water and methanol several times and dried in vacuum at 60 °C for 24 h.

Powders were carefully grounded, pressed in pellets of 8 mm diameter and 1–2 mm thick under 20 MPa. Samples were conserved in a vacuum oven for electrical and magnetic measurements.

Characterization

Wide-angle X-ray scattering of polyaniline composites films were collected on a Rigaku model diffractometer equipped with a copper X-ray tube wavelength (≈0.154 nm). Diffracted intensity was collected for 2θ angle from 5 to 60° with a step 0.05°. Relative crystalline size was estimated for the integral intensity of the X-ray diffraction peak (311) by using Scherer equation:

$$D = k\lambda/\alpha\cos\theta \quad (1)$$

where k is the shape factor, λ is the X-ray wavelength (1.5406 Å), α is the full width at half-maximum expressed in unit of 2θ, and is the Bragg angle (°).

UV–visible spectra was performed in a spectrometer Shimadzu UV-2401 PC working in the spectral range 200–900 nm, on chloroform solutions of the powders finely grounded, For spectroscopic analysis, each solution was conveniently diluted.

Thermogravimetric analysis (TG) of the composites was carried on a thermalgravimetric analyzer (Shimadzu, DTG-50) under a linear heating of 10 K min^{-1}, in air atmosphere.

Transport properties in the range 10–300 K were performed using a physical property measurement system (PPMS) from Quantum Design.

The electrical conductivity of pellets was measured using a standard two-point method. The current was applied by a Keithley Model 220 current source, and the voltage was measured independently by a Hewlett Packard Model 34401A multimeter. Since PANI is hygroscopic, all samples were stored under vacuum until the time of measurement.

Magnetization measurements of composite powders were performed using a superconducting quantum interference device (SQUID) magnetometer (Quantum Design MPMS) at fields ranging from 0 to 1.5 T (15,000 Oe) at temperatures ranging from 5 K to 300 K. For Zero Field Cooled (ZFC) magnetization the sample was cooled to 10 K with the magnetic field set to zero. After stabilization at the low temperature, a weak magnetic field at 50 Oe was applied and the magnetization was measured while the temperature was increased. In the Field cooled (FC) experiments, the sample was cooled at 10 K with the weak magnetic field of 50 Oe applied. The magnetization was measured while stepping the temperature up to 300 K.

Results and discussion

Figure 1 shows the wide-angle X-ray scattering patterns of powders of PANI–DBSA (a) and of samples of Fe_3O_4/PANI–DBSA composite with different Fe_3O_4 content (b–d). The characteristic Fe_3O_4 spectrum obtained from a dried sample (Sect. ''Synthesis of magnetite nanoparticles'') is presented (e). As both, magnetite and maghemite have similar XRD patterns, Mössbauer spectra were performed on samples (not shawn in this work). They show two different magnetic sites with different IS for iron, so we can assume that magnetite is present.

Diffraction patterns of polyaniline with a large molecular weight tend to display a broad amorphous halo over the range 2θ: 10–25° and three distinct peaks at the angles 2θ: 12, 20, 25° [15]. The relative intensity of these peaks might differ, depending on the conditions of the polymerization process. In Fig. 1 these reflections are observed in (a) and in the composites with magnetite content up to 16 wt.% (b, c) with higher intensity, especially the reflection at 20°. The diffraction profile of the spinel structure (magnetite) shows characteristic Bragg's reflections near 2θ: 30.10 (d = 0.297 nm), 35.42 (d = 0.253 nm), 43.20 (d = 0.209 nm), 53.48 (d = 0.171 nm) and 57.94° (d = 0.162 nm). These data are in good agreement with that of Fe_3O_4 [16]. Crystalline size for the as prepared magnetite (Fig. 1e) was estimated in ~11 nm. Obviously, the sharps peaks and their relative intensities observed for Fe_3O_4/PANI–DBSA nanostructures (b–d) are nearly corresponding to those of Fe_3O_4. This indicates that the crystalline structure of Fe_3O_4 is preserved in the composites.

Figure 2 shows the typical transmission electron microscopic (TEM) images of Fe_3O_4/PANI–DBSA nanoparticles for a sample with 2.6 wt.% of Fe_3O_4. An amorphous matrix (PANI–DBSA) is observed where some black dots (Fe_3O_4 particles) in diameter of 10–15 nm (in coincidence with DRX analysis) embedded are observed.

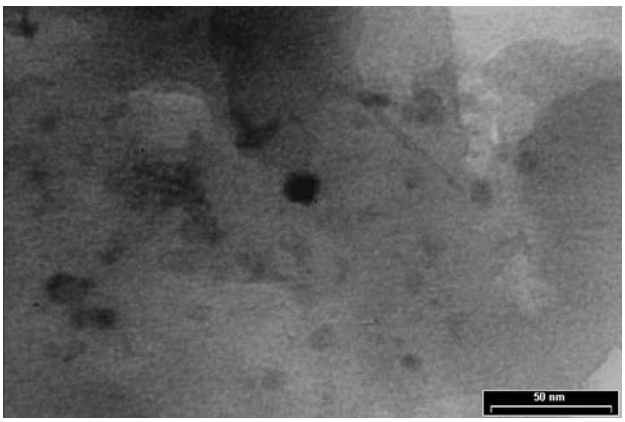

Fig. 2 Transmission electron microscopic images of Fe_3O_4/PANI–DBSA nanoparticles (2.6 wt.% of Fe_3O_4)

Figure 2 also indicates that most of the Fe_3O_4 particles are finely dispersed in the PANI matrix. In fact, it is the polymer matrix that plays the role of minimizing the aggregation of nanoparticles (aggregation is difficult to avoid completely). As mentioned in the experimental section, Fe_3O_4 particles were dispersed in $FeCl_3$ solution so Fe^{3+} was absorbed onto the surface of the Fe_3O_4 particles to form surrounding positively charged (Fe^{3+}) shells. A thin layer of PANI appears on the surface [10]. In order to polymerize the remained aniline monomer, a fixed amount of $FeCl_3$ solution was added, under supersonic stirring, to the reacting solution. As a result, it is possible to form a ''core-shell'' structural mixture, in which Fe_3O_4 nanoparticles are as a ''core'' and the polyaniline as a ''shell''. The resulting composite could dissolve in chloroform.

Figure 3 shows the TGA curves of various Fe_3O_4/PANI–DBSA composite samples. All of them have good

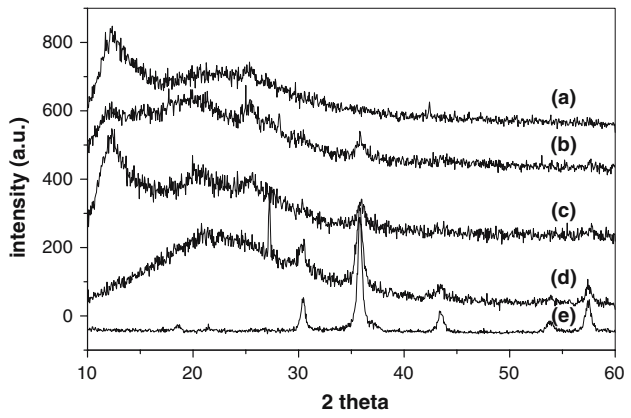

Fig. 1 X-ray scattering patterns of Fe_3O_4/PANI–DBSA powders with different Fe_3O_4 content: (**a**) 0 wt.%, (**b**) 2.6 wt.%, (**c**) 8 wt.%, (**d**) 42 wt.%, and (**e**) Fe_3O_4 nanoparticles as prepared (Sect. ''Synthesis of magnetite nanoparticles'')

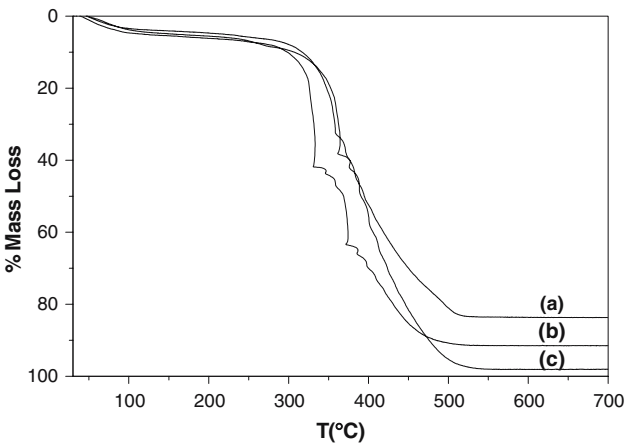

Fig. 3 TGA traces at a heating rate at 10 °C/min in air for various Fe_3O_4/PANI–DBSA composite samples with different Fe_3O_4 content: (**a**) 16.0 wt.%, (**b**) 8.0 wt.%, and (**c**) 2.6 wt.%

thermal stability; the apparent weight loss can be observed only when temperature is over 285 °C. It can be seen that all the samples demonstrate three-stage weight loss, a steady weight loss over the temperature range from room temperature to ~ 120 °C, a sharp falls in specimen weight over the temperature ranges from ~ 285 to 350 °C and from ~ 360 to 520 °C, respectively. The first step (50–120°C) indicates the loss of water in the polymer matrix; the second weight loss may be attributed to loss of acid dopand or volatile elements bound to the polyaniline chain [17]. The third decomposition step occurs between 360 and 520 °C where the mass loss may be due to oxidative degradation of polymer in air. From TGA determination, Fe_3O_4 weight percentage in all samples, was estimated.

UV-spectrometer was used to verify the behavior of PANI/doped/solvent complexes. Figure 4 shows UV–visible spectra of Fe_3O_4/PANI–DBSA composites solutions with different Fe_3O_4 content. The spectrum in chloroform shows the characteristic peak of PANI–DBSA (a) at 360 nm due to $\pi \rightarrow \pi^*$ transition of benzenoid amine structure of PANI and at 860 nm as a result of the excitation of the quinoid imines structure. The solvent protonation is manifested by the presence of a new peak at 440 nm. This transition is usually attributed to the molecular exciton. It corresponds mainly to transition involving the delocalized highest occupied molecular orbital (HOMO) to a virtual orbital which is localized in the quinone-diimine portion of the oligomer, as has been reported by other authors [18]. Characteristic peaks in composite samples are observed at 353–440 and 766, 780 and 807 nm in Fig. 4b–d, respectively. The ~400 nm peak is a result of doped benzenoid amine excitation while the ~800 nm peak is due to the change from polaron to the bipolaron state. In Fig. 4b–d the characteristic peaks are hypsochromically shifted specially the polaron band. This

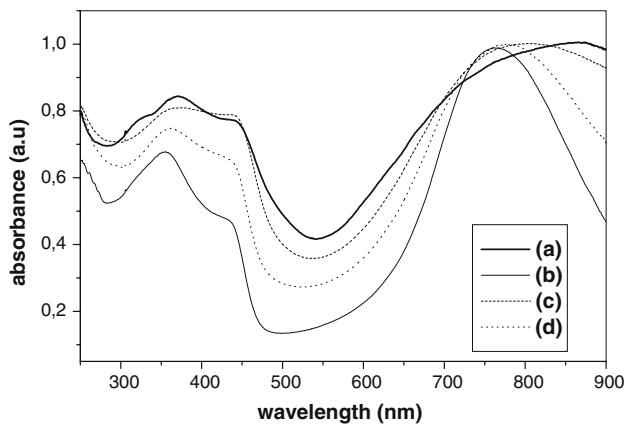

Fig. 4 UV–visible spectra of Fe_3O_4/PANI–DBSA composites solutions with different Fe_3O_4 content: (**a**) 0 wt.%, (**b**) 2.6 wt.%, (**c**) 8.0 wt.%, and (d) 16.0 wt.%

happens because for increasing amount of magnetite, the polymer becomes less compatible with the solvent (Chloroform) and the molecules become increasingly coiled to decrease their contact with the solvent [19]. These results probably indicate that there is some interaction between Fe_3O_4 particles and PANI backbone as was earlier reported by us from infrared measures [8]. Interaction between magnetic nanoparticles and polymer bone is supported by IR analysis (not shown in the manuscript)

A commonly used technique for the investigation of superparamagnetic relaxation is the FC–ZFC magnetization in a weak applied field as a function of increasing temperature. The ZFC–FC curves for pure Fe_3O_4 nanoparticles (a) and for Fe_3O_4/PANI composite samples (b and c) measured in a field of 50 Oe, are shown in Fig. 5. As a general observation we note that the magnetic behavior displayed is typical for fine particles system where the relaxation of the magnetic moment of the particles is present. In the ZFC process, at the lowest temperatures, the total magnetic moment is nearly zero due to freezing of the moments in random directions. As the temperature is raised, the total magnetic moment increases due to the gradual alignment of moments in the field direction until it reaches the maximum value (T_b). We note that for our samples we could not observe a very well defined maximum of the ZFC curves in pure Fe_3O_4 nanoparticles (Fig. 5a) and for composite samples containing over 36 wt.% Fe_3O_4 (Fig. 5c) where magnetic dipolar interactions are present. In Fig. 5b (16 wt.% Fe_3O_4) the magnetization increases monotonically with decreasing temperature in the FC case indicative of the presence of ultrafine superparamagnetic particles in the sample. This effect is not observed in Fig. 5a and c. The ZFC magnetization curve, however, separates from the FC curve and passes through a maximum at 195 K (T_b). The broadness of the peak maximum of the ZFC curve clearly shows that the nanoparticles are polydisperse in size. The polyaniline matrix allows each ferrite nanoparticles to behave independently and interparticle interactions are not important. For the shape of the curves a very clear trend of the variation of the blocking temperature with the concentration of the magnetic nanocrystal in the polymer can be deduced. As the concentration of the magnetic nanoparticles in the nanocomposite increases, the blocking temperature increases [20].

Figure 6 shows the reduced magnetization (M/M_s) versus applied magnetic field (H) at 300 K for a Fe_3O_4/PANI (2.6 wt.% Fe_3O_4) composite sample. When grain size of magnetite particles decreases to a critical size (<20 nm), the coercive force H_c decreases to zero and the nanoparticles exhibit a superparamagnetic behavior, which can be usually observed at room temperature (above blocking temperature) [21]. The applied magnetic field H dependence

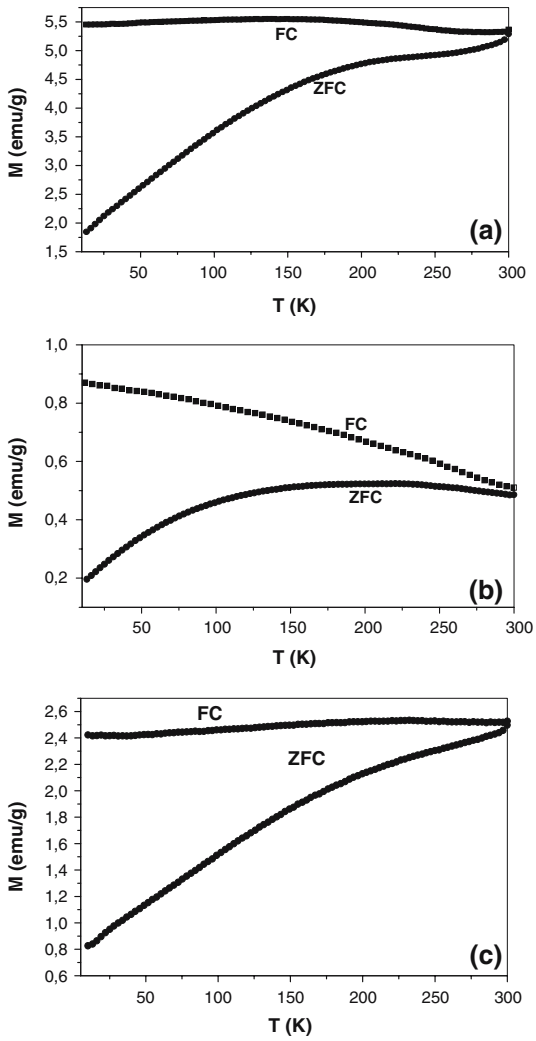

Fig. 5 The ZFC and FC curves for (**a**) Fe_3O_4 nanoparticles, (**b**) Fe_3O_4/PANI (16 wt.% Fe_3O_4), and (**c**) Fe_3O_4/PANI (32 wt.% Fe_3O_4) composite samples

of the magnetization M can be described by Langevin equation [22]

$$M = M_s[\coth(\mu H/kT - kT/\mu H)]$$

where M and M_s are the magnetization and the saturation magnetization (emu cgs) respectively,

$$\mu = \frac{M_s \pi \rho D^3}{6} \quad (3)$$

μ is the magnetic moment of each particle (emu cgs), H is the magnetic field (Oe), T is the absolute temperature, and k is the Boltzmann constant. The Langevin relation considers each particle as a magnetic monodomain. Figure 6 shows the best fit for the Langevin function in Eq. (2). From this data fitting, the mean-magnetic moment per particle of sample is found to be 2,529 μ_B (Eq. (3)). The relationship

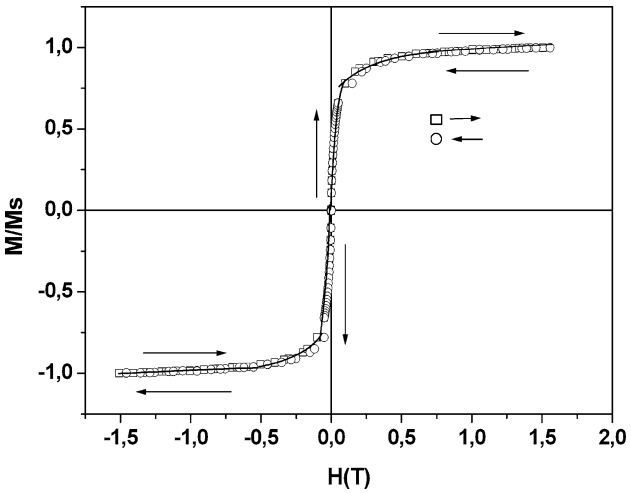

Fig. 6 Reduced magnetization (M/M_s) versus applied magnetic field (H) at 300 K for a Fe_3O_4/PANI (2.6 wt.% Fe_3O_4) composite sample

between the magnetic moment and the particle diameter is given by the following equation.

$$D = \sqrt{[3]}\frac{6\mu}{M_s \pi \rho}$$

The particle diameter results in the order of 12.1 ± 0.3 nm, in agreement to TEM images and with DRX analysis.

Magnetization versus magnetic field curves for a sample of Fe_3O_4/PANI–DBSA composite (2.6 wt.% of Fe_3O_4) at different temperature are shown in Fig. 7. The inset shows the variation of the sample magnetization at 0.1 T when the temperature changes in the range 5–300 K. The absolute increase of the magnetization at 5 K compare to room

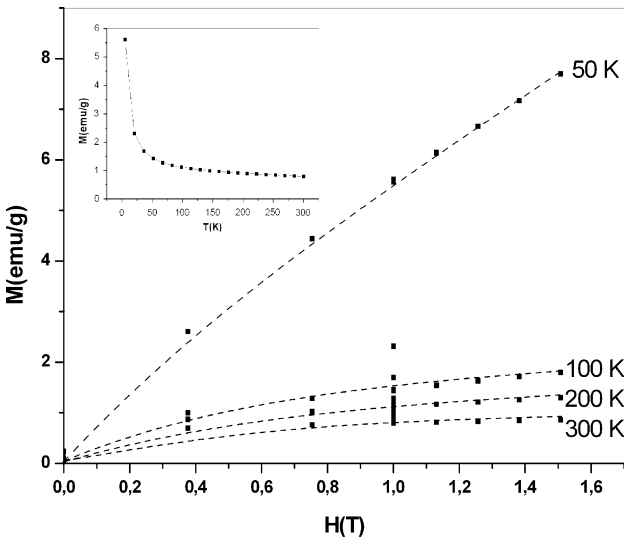

Fig. 7 Magnetization curves at different temperature (5, 50, 100 and 300 K) for a sample of Fe_3O_4/PANI composite with 2.6 wt.% of Fe_3O_4 nanoparticles. Inset: the variation of the sample magnetization at 0.1 T with temperature

temperature shows a typical behavior of ferromagnetic materials and can be reasonable considered as a result of decrease in thermal energy [23].

Application of a magnetic field will align the magnetic moment of the nanoparticles in the field direction, and magnetization rises with increasing field until, in many cases, a saturation value is reached. When a magnetic field is applied to the Fe_3O_4/PANI–DBSA composite at 300 K (2.6 wt.% of Fe_3O_4), the magnetization increases rapidly and reaches 0.87 emu/g Fe_3O_4 at an applied magnetic field of 1.5 T (Fig. 7). As the temperature is lowered, the magnetization increases. At 5 K, similarly, the magnetization of the nanocomposite increases with increasing field, but in this case, the magnetization continuously increases without saturation. The maximum magnetization at low temperature which is higher than that of the composite at room temperature is still lower than the saturation magnetization (84 emu/g) for bulk Fe_3O_4 particle [22] and 65 emu/g for Fe_3O_4 nanoparticles [24] (Table 1).

In Fig. 8 the influence of the Fe_3O_4 content on the saturated magnetization (M_s) of the Fe_3O_4/PANI composites is shown. When the Fe_3O_4 content increases from 0.3 to 100%, the saturated magnetization linearly increase from 0.167 to 59.38 emu/g.

The weaker magnetization and lack of saturation have often been observed in ferromagnetic iron oxides nanoparticles of similar sizes due to the surface and size effects

Table 1 Magnetization at 1.5 T (M_s) and coercive force (H_c) at different temperature for a sample of Fe_3O_4/PANI composite with 2.6 wt.% of Fe_3O_4 nanoparticles

T (K)	300	100	50	5
M_s (emu/g)	0.87	1.29	1.80	7.71
H_c (T)	~0	25.6	79.6	160

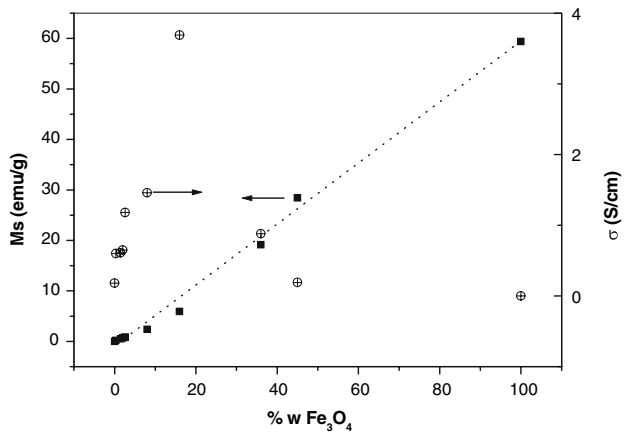

Fig. 8 Magnetization at 1.5 T (M_s) and conductivity (σ) at 300 K for samples of Fe_3O_4/PANI composite with different Fe_3O_4 content

[25, 26]. The discontinuity of the superexchange bonds between the iron cations near/on the nanoparticles surfaces leads to the formation of canted spins. The no collinear spin structure due to the pinning of the surface spins at the interface of the magnetic nanoparticles and the polyaniline coating reduces the total magnetic moment of the nanoparticles. The distribution in the nanoparticles size and the superparamagnetic relaxation of the smaller particles in the distribution leads to the no saturation of the magnetization.

At room temperature, the conductivity of Fe_3O_4/PANI composites increased from 0.18 to 3.69 S/cm when the content of Fe_3O_4 varied from 0 to 16% (Fig. 8). At the point of 16%, the conductivity reached the maximum value. Then, the conductivity of Fe_3O_4/PANI composites reduced with the increase of the Fe_3O_4 content. This phenomenon was accordant with some other references [27–29]. In the disordered system like the conducting polymers, microscopic conductivity depends upon the doping level, conjugation length or chain length while the macroscopic conductivity depends on some external factors like compactness of the sample, orientation of the microparticles, etc. In our composites, on the one hand, the intrinsic microscopic conductivities are more or less equal, because of the PANI being polymerized in identical conditions. On the other hand, as the PANI content in the composites lowered, the change in compactness becomes more significant, so the compactness of the Fe_3O_4/PANI particles in the composite improved with the Fe_3O_4 content in the system. As a result, the weak links between the grains are increasingly improved and the coupling through the grain boundaries becomes stronger. Similar results have been reported for Co_3O_4/PANI and TiO_2/PANI composites [30]. For higher Fe_3O_4 content (>16 wt.%), the decrease in conductivity may be due to particle blockage of conduction path by the Fe_3O_4 nanoparticles embedded in the PANI matrix.

The temperature dependent of resistivity of PANI/Fe_3O_4 composites with different Fe_3O_4 content was measured at temperature between 10 K and 300 K. The conductivity of all measured samples decreased with decreasing temperature exhibiting typical semiconducting behavior as shown in Fig. 9. Further studies are in progress.

Conclusions

- We successfully synthesized polyaniline (PANI) composites containing Fe_3O_4 nanoparticles (about 10–13 nm) by ''in situ'' polymerization in the presence of DBSA and HCl as a dopant.
- The Fe_3O_4/PANI nanocomposite prepared in a single step, with good solubility in organic solvents, exhibited high conductivity and magnetic properties.

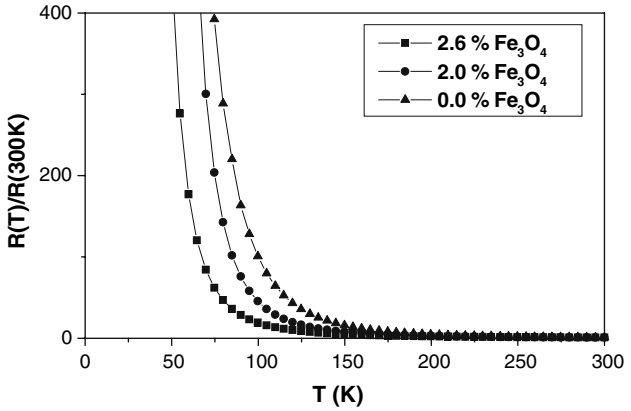

Fig. 9 Temperature dependence of resistivity of conducting polymer-composites with different Fe_3O_4 content

- Zero field cooling and FC profiles showed that the polyaniline matrix allows each ferrite nanoparticles to behave independently and interparticle interactions are not important for iron oxide content lower than 36 wt.%.
- The conductivity of PANI can be remarkably heightened in the presence of Fe_3O_4. The conductivity at room temperature of the composite (16 wt.%) has reached 3.7 S/cm.
- Samples exhibit typical semiconducting behavior

Free standing Fe_3O_4/PANI nanocomposite films can be prepared by the controlled evaporation of the solvents of the mixture suspensions cast onto glass plates at room temperature. Magnetic and electric properties of these films are in progress.

Acknowledgements The authors thank Dr. Troiani (CAB-CNEA) for TEM images. This work is supported by the University of Buenos Aires (grant I–055).

References

1. Kawaguchi H (2000) Prog Polym Sci 25(8):1171
2. Gómez-Romero P (2001) Adv Mater 13(3):163
3. Marchessault RH, Rioux P, Raymond L (1992) Polymer 33(19):4024
4. Wan M, Zhou W, Li J (1996) Synth Met 78:27
5. Lin J, Wan MX (2000) J Polym Sci Part A Polym Chem 38(15):2734
6. Zhang Z, Wan M (2003) Synth Met 132:205
7. Wan MX, Li J (1997) J Polym Sci Part A 35(11):2129
8. Aphesteguy J, Jacobo S (2004) Physica B 354(1–4):224
9. Long Y, Chen Z, Duvail J, Zhang Z, Wan M (2005) Physica B 370:121
10. Chen A, Wang H, Zhao B, Li X (2003) Synth Met 139:411
11. Cao Y, Smith P, Heeger AJ (1992) Synth Met 48:91
12. Cao Y, Smith P (1993) Polymer 34:3139
13. Gustafsson G, Cao Y, Treac GM, Klavetter F, Colaneri N, Heeger AJ (1992) Nature 357:477
14. Yin W, Ruckenstein E (2000) Synth Met 108:39
15. Laska J, Widlarz J (2005) Polymer 46:1485
16. JCPPS Power Diffraction File International Center for Diffraction Data (1980) Fe_3O_4, Newtown Square, PA
17. Wang XH, Geng YH, Wang LX, Jing XB, Wang FS (1995) Synth Met 69:265
18. Liebert J, Cornil J, Dos Santos DA, Brédas J (1997) Phys Rev B 56(14):8638
19. Zhang W, Min Y, MacDiarmid AG, Angelopoulos M, Liao YH, Epstein AJ (1997) Synth Met 84:109
20. Sunderland K, Brunetti P, Spinu L, Fang J, Wang Z, Lu W (2004) Mater Lett 58:3136
21. Tang B, Geng Y, Sun Q, Zang X, Jing X (2000) Pure Appl Chem 72:157
22. Cornell RM, Schwertmann U (1996) The iron oxides. VCH, Weinheim
23. Chen DH, Chen YY (2002) Mater Res Bull 37:801
24. Zhang Z, Wan M (2003) Synth Met 132:205
25. Nguyen T, Diaz A (1994) Adv Mater 6:858
26. Zhang L, Papaefthymiou G, Ying J (1997) J Appl Phys 81:6892
27. Gangopadhyay R, De A (1999) Eur Polym J 35:1985
28. Chen A, Wang H, Li X (2004) Synth Met 145:153
29. Zhang L, Wan M (2003) J Phys Chem B 107:6748
30. Su S, Kuramoto N (2000) Synth Met 114:147